Surface-enhanced Raman scattering at a planar dielectric interface beyond critical angle

Denis Pristinski,[1,2] Eric C. Le Ru,[3] Siliu Tan,[1] Svetlana Sukhishvili,[4] and Henry Du[1,*]

[1]*Department of Chemical Engineering and Materials Science, Stevens Institute of Technology, Hoboken, NJ 07030, USA*

[2]*Currently with Polymers Division, National Institute of Standards and Technology, Gaithersburg, MD 20899, USA*

[3] *The MacDiarmid Institute for Advanced Materials and Nanotechnology, School of Chemical and Physical Sciences, Victoria University of Wellington, P.O. Box 600,, Wellington, New Zealand*

[4]*Department of Chemistry, Chemical Biology, and Biomedical Engineering, Stevens Institute of Technology, Hoboken, NJ 07030, USA*

[*]*Corresponding author: Henry.Du@stevens.edu*

Abstract: Light refraction at the planar boundary of dielectric media prevents light propagation in the higher refractive index medium at angles beyond the critical value. This limitation is lifted when the evanescent wave is excited at the lower refractive index side of the interface. In this work we quantify polarization and angle dependence of surface-enhanced Raman scattering (SERS) intensity beyond the critical angle. Specifically, Raman spectra of thiocyanate molecules adsorbed on clustered silver nanoparticles at the water-glass interface were acquired using evanescent excitation and detection. Detected SERS signal polarization and scattering angle dependence are shown to be in agreement with a simple model based on excitation and radiation of a classical dipole near a lossless interface.

OCIS codes: (240.6695) Optics at surfaces; (260.6970) Physical optics; (240.6490) Spectroscopy, surface.

References and links

1. L. Novotny, "Allowed and forbidden light in near-field optics," J. Opt. Soc. Am. A **14**, 91–114 (1997).
2. C. K. Carniglia, L. Mandel, and K. H. Drexhage, "Absorption and emission of evanescent photons," J. Opt. Soc. Am. A **62**, 479–486 (1971).
3. A. L. J. Burgmans, M. F. H. Schuurmans, and B. Bölger, "Transient behavior of optically excited vapor atoms near a solid interface as observed in evanescent wave emission," Phys. Rev. A **16**, 2002–2007 (1977).
4. H. H. Choi, H. J. Kim, J. Noh, C.-W. Lee, and W. Jhe, "Measurement of angular distribution of radiation from dye molecules coupled to evanescent wave," Phys. Rev. A **66**, 053803 (2002).
5. T. Matsudo, H. Hori, T. Inoue, H. Iwata, Y. Inoue, and T. Sakurai, "Direct detection of evanescent electromagnetic waves at a planar dielectric surface by laser atomic spectroscopy," Phys. Rev. A **55**, 2406–2412 (1997).
6. T. Inoue and H. Hory, "Quantization of evanescent electromagnetic waves based on detector modes," Phys. Rev. A **63**, 063805, (2001).
7. L. Luan, P. R. Sievert and J. B. Ketterson, "Near-field and far-field electric dipole radiation in the vicinity of a planar dielectric half space," New J. Phys. **8,** 264 (2006).
8. G. Videen, "Light scattering from a sphere behind a surface," J. Opt. Soc. Am. A **10**, 110–117 (1993).
9. M. J. Jory, E. A. Perkins, J. R. Sambles, "Light scattering by microscopic spheres behind a glass–air interface," J. Opt. Soc. Am. A **20**, 1589–1594 (2003).
10. M. J. Jory, P. S. Cann, J. R. Sambles, and E. A. Perkins, "Surface-plasmon-enhanced light scattering from microscopic spheres," Appl. Phys. Lett. **83**, 3006–3008 (2003).
11. M. Moskovits, "Surface-enhanced spectroscopy," Rev. Mod. Phys. **57**, 783–826 (1985).
12. G. C. Schatz, M. A. Young, and R. P. Van Duyne, "Electromagnetic mechanism of SERS," Top. Appl. Phys. **103**, 19–46 (2006).
13. E. C. Le Ru and P. G. Etchegoin, "Rigorous justification of the $|E|^4$ enhancement factor in Surface Enhanced Raman Spectroscopy," Chem. Phys. Lett. **423**, 63–66 (2006).
14. H. Xu, J. Aizpurua, M. Käll, and P. Apell, "Electromagnetic contributions to single-molecule sensitivity in surface-enhanced Raman scattering," Phys. Rev. E **62**, 4318–4324 (2000).

#102014 - $15.00 USD Received 26 Sep 2008; revised 11 Nov 2008; accepted 12 Nov 2008; published 21 Nov 2008

15. E. C. Le Ru, M. Meyer, E. Blackie, and P. G. Etchegoin, "Advanced aspects of electromagnetic SERS enhancement factors at a hot-spot," J. Raman Spectrosc. **39**, 1127–1134 (2008).
16. H. Du, R. Bise, C. Christodoulatos, H-L. Cui, and S. A. Sukhisvili, "Photonic Crystal Fibers with Nanoscale Functionalized Air Holes as Robust Chemical and Biological Sensors," NSF Nanoscale Sci. and Eng. Grantees Conf. 0404002 (2005).
17. J. P. Goudonnet, T. Inagaki, E. T. Arakawa, ant T. L. Ferrell, "Angular and polarization dependence of surface-enhanced Raman scattering in attenuated-total-reflection geometry," Phys. Rev. B **36**, 917–921 (1987).
18. S. Tan, M. Erol, A. Attygalle, H. Du, and S. Sukhishvili, "Synthesis of positively charged silver nanoparticles via photoreduction of $AgNO_3$ in branched polyethyleneimine/HEPES solutions," Langmuir **23**, 9836–9843 (2007).
19. J. Mertz, "Radiative absorption, fluorescence, and scattering of a classical dipole near a lossless interface: a unified description," J. Opt. Soc. Am. B **17**, 1906–1913 (2000).
20. E. C. Le Ru, M. Meyer, P. G. Etchegoin, "Proof of Single-Molecule Sensitivity in Surface Enhanced Raman Scattering (SERS) by Means of a Two-Analyte Technique," J. Phys. Chem. B **110**, 1944–1948 (2006).
21. E. C. Le Ru, P. G. Etchegoin, and M. Meyer, "Enhancement factor distribution around a single SERS hot-spot and its relation to single molecule detection," J. Chem. Phys. **125**, 204701 (2006).

1. Introduction

We report on the angle-resolved detection of the light inelastically scattered by thiocyanate molecules adsorbed on silver nanoparticles beyond the critical angle at the glass-water interface. Light crossing the planar boundary between two dielectric media experiences refraction and in the medium having higher refractive index light propagation is confined below the critical angle. However, in the vicinity of the interface, light emitted as an evanescent wave in the lower refractive index medium will propagate in the other medium at an angle beyond the critical one [1]. This effect, which is an inverse of total internal reflection, was demonstrated for luminescent emission at solid-liquid [2] and solid-gas [3] interfaces using normal incidence excitation, and later at solid-liquid [4] and solid-gas [5] interfaces using evanescent field excitation. The latter two results were shown to be in good agreement with a quantum mechanical treatment of electric dipole radiation near dielectric surfaces [6]. A detailed simulation of radiation patterns with similar geometry based on Sommerfeld formalism was published recently [7].

When an emitting dipole is replaced with a light scattering sphere, multiple reflections between media boundary and sphere surface have to be taken into account. In this case, extended Mie theory was shown to provide general solution in the form of angle-dependent Mueller matrix [8]. The theory was experimentally tested measuring light scattered by glass microspheres at the air–glass interface below the critical angle [9] and the scattering was then enhanced by introducing a thin gold film on top of the glass and achieving surface plasmon resonance [10]. In the case of surface-enhanced Raman scattering (SERS), the excited surface plasmons are localized and, while the electromagnetic contribution to enhancement is well understood [11–13], including the influence of hot spots [14,15], the theory was not extended until now to quantify the evanescent wave excitation by SERS.

The relevant geometry of applications that utilizes the interaction of evanescent wave with localized surface plasmons is an optical lightguide covered with a SERS-active substance used as a spectroscopic sensor. One promising example is a solid-core photonic crystal fiber (PCF) with its cladding air channels containing immobilized gold or silver nanoparticles along the fiber length [16]. Long interaction path length can potentially increase signal intensity and improve reproducibility. However, this kind of sensor can only collect and guide the light scattered at angles above the critical value and therefore involving the emission of evanescent waves. While evanescent wave excitation was successfully used for angle-resolved SERS detection [17], it is the ability of the lightguide to collect scattered light which we evaluate for the first time.

#102014 - $15.00 USD Received 26 Sep 2008; revised 11 Nov 2008; accepted 12 Nov 2008; published 21 Nov 2008

2. Experimental setup

The setup geometry was similar to a surface plasmon resonance arrangement and is depicted in Fig. 1. A 1 mm diameter linearly polarized laser beam (diode pumped solid state laser, 200 mW stabilized power, 532 nm wavelength) came through a zero-order quarter-wave plate and a Glan laser calcite polarizer mounted on rotary stages. The beam was refracted at one side of a right angle uncoated borosilicate glass prism (refractive index $n = 1.52$) and was incident on its base at the angle ~72.7°. Total internal reflected beam exited from the opposite side of the prism; the exiting beam power was in the range from 75 to 90 mW depending on its polarization. Below, *S*-polarization refers to the light polarized in the interface plane (TE mode), and *P*-polarization refers to the light polarized in the plane of incidence (TM mode). The base of the prism served as the bottom of a cylindrical liquid cell. Sample substrate preparation is described later in the text. The scattered light collection optics was mounted on a goniometer stage and could be positioned above or below the reflected laser light. The rotating axle of the stage could also transit up and down to account for the refraction of light exiting the prism. The aperture behind the collimating lens (achromatic doublet, $f = 25$ mm) was set to obtain the full collection angle of ~3.6° in the air. Accordingly, the goniometer was rotated by 3° between the measured points. The collimated scattered light went through a notch filter (O.D. = 4.0, 150 cm^{-1} edge width), another Glen laser polarizer, and was coupled to a 100 µm core diameter multimode fiber using $f = 8$ mm aspheric glass lens. The fiber was connected to a 0.3 m spectrometer with a 25 µm entrance slit, a 600/mm grating, and a liquid nitrogen cooled CCD camera with 25×25 µm pixel size and 1024×256 pixels.

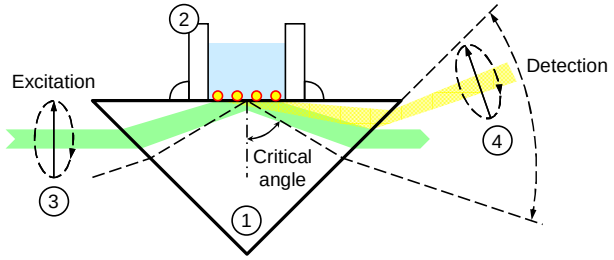

Fig. 1. Schematic of experimental setup: (1) right angle glass prism, (2) glass cylinder glued on top of the prism, (3) rotating polarizer following the laser, (4) rotating polarizer preceding the spectrometer.

The described geometry reproduces the single reflection of light propagating along the solid silica core of modified photonic crystal fiber (PCF) having its air cladding filled with analyte solution. A guided mode inside the PCF extends into solution similarly to the evanescent field at the solution side of the flat interface. The detection of light scattered beyond the critical angle would directly indicate the capability of the PCF core to collect the SERS signal resulting from the evanescent field excitation.

3. Substrate characterization

Clustered silver nanoparticles were chosen for their exceptional Raman signal enhancement ability due to a number of 'hot spots' available between the aggregated particles. Positively charged silver nanoparticles were prepared by photo reduction of silver nitrate using branched polyethyleneimine in HEPES buffer solution [18]. Cell glass surface was first coated by gelatin using 0.2 mg/ml gelatin solution in pH 5 adjusted water for 30 min at room temperature. Silver nanoparticles were then deposited to the walls and the bottom of the cell from pH 7.2 HEPES buffered solution for 24 hrs. Particles formed nano-clusters, as shown in the SEM micrographs in Fig. 2. At shorter deposition times no clusters were formed and SERS enhancement from individual nanoparticles was not sufficient to obtain reproducible narrow angle resolved spectra. As one can see, particles have wide size distribution but the average Ag particle size is below the calculated 73 nm evanescent field penetration depth.

#102014 - $15.00 USD Received 26 Sep 2008; revised 11 Nov 2008; accepted 12 Nov 2008; published 21 Nov 2008

Finally, the rinsed cell was filled up with 1 ppm SCN^- solution in DI water and sealed with Parafilm. Control samples using cover glasses as a cell bottom for microscope based SERS spectroscopy demonstrated strong and stable C≡N vibration Raman peak at ~2105 cm^{-1} used for the measurements reported.

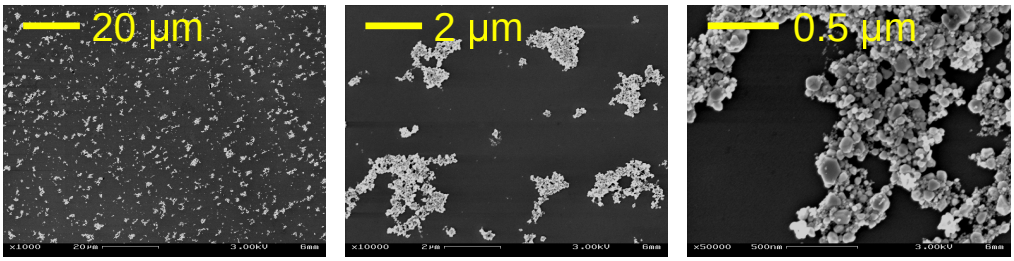

Fig. 2. SEM images of clustered silver nanoparticles deposited on silicon substrate following the surface modification procedure described in the text. Images are shown for the same substrate at different magnification.

The raw spectra for *S* excitation and detection polarization are presented in Fig. 3. In contrast with luminescence measurements, the direct intensity detection using an appropriate narrow bandpass filter was impossible due to a very low signal-to-background ratio. For each spectrum, background subtraction was applied before estimating the Raman peak intensity. The prism was mounted on XY transition stage and the SERS signal was found to be uniform across the cell bottom surface. No C≡N peak intensity decay was observed on freshly prepared substrates within the first 6 hrs of measurements, however the peak height noticeably decreased after 24 hrs.

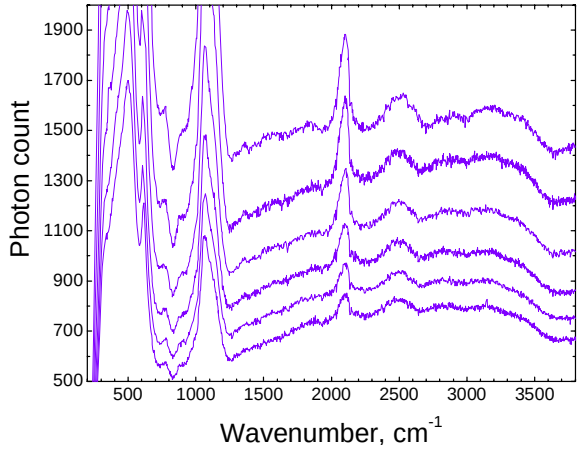

Fig. 3. SERS spectra of SCN^- molecules adsorbed on nanoparticle Ag clusters at water-glass interface for different scattering angles in the range from 74° (top spectrum) to 81° (bottom spectrum). Both excitation and detection were for *S*-polarized light. Exposure time was 2 min. Peaks below 1300 cm^{-1} are from borosilicate glass.

4. Geometrical corrections

To recover relative intensities of Raman signal for all polarizations and scattering angles, the following geometrical corrections had to be applied. Light entering and exiting the prism was partially reflected at the air-glass interface, as schematically shown in Fig. 4(a). The reflection coefficients are polarization and angle dependent and, for the case of uncoated glass, described by Fresnel equations:

#102014 - $15.00 USD Received 26 Sep 2008; revised 11 Nov 2008; accepted 12 Nov 2008; published 21 Nov 2008

$$R^S = \left(\frac{n_G \cos\alpha_G - \cos\alpha_A}{n_G \cos\alpha_G + \cos\alpha_A} \right)^2, \quad R^P = \left(\frac{\cos\alpha_G - n_G \cos\alpha_A}{\cos\alpha_G + n_G \cos\alpha_A} \right)^2, \tag{1}$$

Where, for the scattered light exiting the prism, $\alpha_G = \theta - \pi/4$ is the angle between the light beam at the glass side and the normal to the prism side surface, $\alpha_A = \sin^{-1}(n_G \sin\alpha_G)$ is the angle between the light beam at the air side and the normal to the prism side surface, n_G is the prism glass refractive index (1.52), and θ is the scattering angle. For the excitation light entering the prism all angles remained fixed: $\theta' = 72.7°$, $\alpha'_G = 27.7°$, and $\alpha'_P = 45°$.

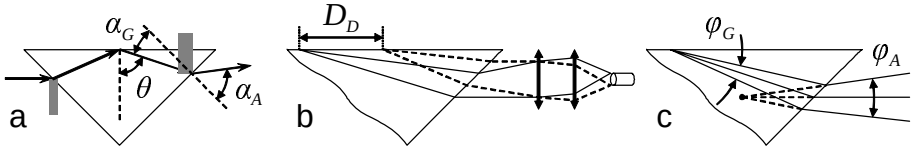

Fig. 4. Schematic of scattering angle dependent geometrical corrections for the right angle prism geometry: (A) partial light reflection, (B) limited sampled area, (C) finite collection angle; see text for more details.

Moreover, the laser used for excitation had 1 mm beam diameter at $1/e^2$ intensity. Following the beam refraction at the left side surface of the prism, the beam profile became elliptical with the major axis of 1.25 mm at $1/e^2$ intensity and, projected to the prism top surface, excited an elliptical spot with the major axis $D_E = 4.22$ mm at $1/e^2$ intensity. For the Gaussian excitation light intensity profile, the amount of scattered light being detected was proportional to $\mathrm{erf}(\sqrt{2}\, D_D / D_E)$, where D_D is the major axis of an elliptical sampled area, as shown in Fig 4(b), which varies with the scattering angle and can be calculated as:

$$D_D = D_0 \frac{\cos\alpha_G}{\cos\theta \cos\alpha_A}, \tag{2}$$

where D_0 is the diameter of the projection of a collecting fiber core to the image plane in the absence of the prism. For 100 μm fiber core diameter and ×0.32 collection system magnification, $D_0 = 0.3125$ mm. This correction is approximate, as it does not account for the change of collimating lens effective focal distance, and therefore system magnification, due to the presence of the prism.

Finally, the solid angle in which the Raman signal was collected also varied with the scattering angle. The collimator lens, having a 25 mm focal distance and a 1.55 mm aperture, collected light within the full angle $\varphi_A = 3.55°$ in the air. Tracing the marginal rays at angles $\alpha_A \pm \varphi_A/2$ refracting at the right side of the prism provides the actual collection angle in the glass as shown in Fig. 4(c). In the plane of incidence:

$$\varphi_G = \sin^{-1}\left(\frac{\sin(\alpha_A + \varphi_A/2)}{n_G} \right) - \sin^{-1}\left(\frac{\sin(\alpha_A - \varphi_A/2)}{n_G} \right). \tag{3}$$

We assume that the scattered light intensity detected is proportional to φ_G which varies between 0.8º and 2.2º for the data presented below. This is also an approximation, which does not account for small changes of collection angle across the sampled area. However, it has to be noted that small (±2 mm) intentional changes of focus at the smallest and the largest detection angles resulted in no signal intensity change, which indicates that a more accurate

#102014 - $15.00 USD Received 26 Sep 2008; revised 11 Nov 2008; accepted 12 Nov 2008; published 21 Nov 2008

ray tracing approach to geometrical corrections would not increase the actual measurement accuracy.

For every detection angle there were five measurements done, four corresponding to the combination of *S* and *P* polarizations of the excitation and detected signal, the fifth measurement was done with polarizers removed. For each angle the position of the goniometer stage was adjusted in the vertical direction to account for the shift of an image of the substrate due to light refraction. The adjustment was done manually, maximizing the signal while the calculated value of the required adjustment was only used as a guiding number.

5. Experimental results

Figure 5 shows the angular dependence of the SERS signal obtained from thiocyanate molecules on silver nano-clusters excited with circularly polarized evanescent light at the glass-water interface and detected beyond the critical angle. The experiment was run three times at different spots on the same substrate and the averaged values and standard deviations are plotted. Measurement was not possible close to the excitation angle as the laser power was above the damage threshold of the notch filter and the output laser beam had to be spatially blocked. Note that 3° rotation of the goniometer stage corresponds to smaller, 1° to 2° change of the actual scattering angle inside the prism. As one can see there is a measurable signal present as far as 22° beyond the critical angle. This result demonstrates the feasibility of using an optical lightguide to collect SERS signal originating from the interaction of the evanescent field with metal nanoparticles at its surface.

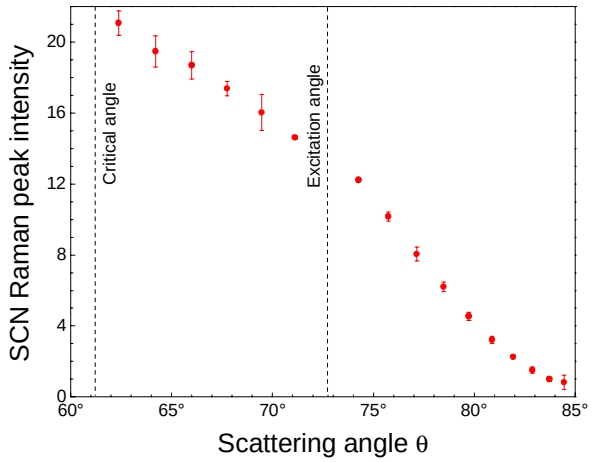

Fig. 5. Angular dependence of SERS signal from SCN^- molecules adsorbed on nanoparticle Ag clusters at water-glass interface beyond the critical angle for the circularly polarized evanescent excitation. Error bars represent standard deviation from three independent runs.

The angular and polarization dependence of the SERS signal from the same sample is presented in Fig. 6. We observed a strong dependence of the signal on excitation and detection polarizations, *S*-polarization being move favorable for both. One can also see that for the case of *P*-polarization for excitation and detection, the C≡N peak could not be accurately measured at scattering angles above 68º. These results are in contrast with only 5º observed angular range and less than 30% overall variation of polarization dependence for evanescently excited and detected fluorescence [4,5] and, as we will show, are specific to surface-enhanced spectroscopy situations where the origin of the signal is localized close to the interface.

#102014 - $15.00 USD Received 26 Sep 2008; revised 11 Nov 2008; accepted 12 Nov 2008; published 21 Nov 2008

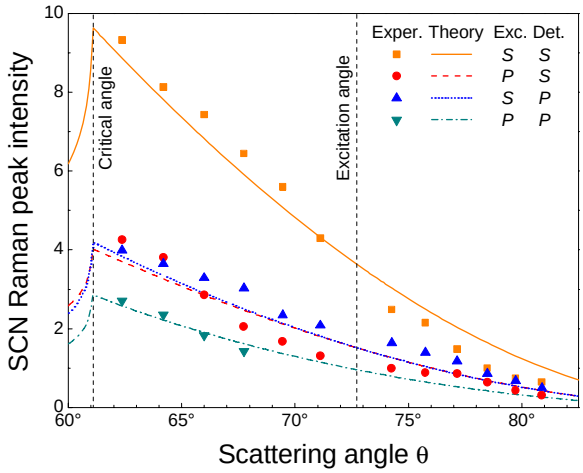

Fig. 6. Angular dependences of SERS signal from SCN^- molecules adsorbed on nanoparticle Ag clusters at water-glass interface beyond the critical angle for *S*- and *P*-polarized evanescent excitation and detection, experimental data (symbols) and theoretical fit (lines).

5. Theoretical model and discussion

We describe in the following a simple theoretical model to explain the observed results and the discrepancies with previous fluorescence experiments. We will assume that the presence of the colloids on the interface does not significantly affect the EM reflection/refraction problem at the prism (n_G) / water (n_W) interface. The normalized electric field (with respect to incident field in the prism) created at a distance d above the prism for *S*- or *P*-polarized excitation and angle of incidence θ then takes the form (ignoring phase factors):

$$\mathbf{E}^S = E_y^S \mathbf{e}_y \exp(-d/2L) \text{ and } \mathbf{E}^P = \left(E_x^P \mathbf{e}_x + E_z^P \mathbf{e}_z\right)\exp(-d/2L), \quad (4)$$

where the complex field components at $d = 0$ derive from the Fresnel transmission coefficients, t^S and t^P, of the interface:

$$E_y^S(\theta) = t^S(\theta), \quad E_x^P(\theta) = \left[2 - t^P(\theta)\right]\cos\theta, \quad E_z^P(\theta) = -\left(n_G^2/n_W^2\right)t^P(\theta)\sin\theta, \quad (5)$$

and the evanescent field penetration depth is $L = (\lambda/4\pi)\left(n_G^2 \sin^2\theta - n_W^2\right)^{-1/2}$ for $\theta > \theta_{crit}$, while $1/L = 0$ for $\theta < \theta_{crit}$.

It is this modified electric field that excites the SERS signal in the colloidal aggregates on the surface. To model the emission of the Stokes-shifted Raman photons at scattering angle θ_R, we apply the Optical Reciprocity Theorem (ORT) as described in Refs. [13,19]. The expressions for the electric field given above can then be used, but with $\theta = -\theta_R$ to account for the forward-scattering geometry (rather than back-scattering) as shown in Fig. 1.

We assume that the SERS signal is dominated by the molecules located at hot spots, typically at the junction between two particles [14]. Such an assumption is appropriate for aggregated colloids as used here [20,21]. Such EM hot spots are highly uni-axial and couple like a dipole to the incident field [15]. Denoting $\mathbf{e}_{HS}$, the unit vector of a hot spot axis, the SERS intensity for a given excitation/detection configuration *ED* (*E* = *S* or *P*, and *D* = *S* or *P*) is then proportional to:

#102014 - $15.00 USD Received 26 Sep 2008; revised 11 Nov 2008; accepted 12 Nov 2008; published 21 Nov 2008

$$I^{ED} = F\left|\mathbf{e}_{HS}\cdot\mathbf{E}^{E}(\lambda_I,\theta_I)\right|^2\left|\mathbf{e}_{HS}\cdot\mathbf{E}^{D}(\lambda_R,-\theta_R)\right|^2, \tag{6}$$

where F characterizes the strength of the hot-spot and is independent of incident and scattering angles and light polarization [15,21] and the indices are for incident (I) and Raman (R) light. Since a large number of hot spots are sampled simultaneously, the measured SERS intensity is proportional to the average of Eq. (6) over all hot spots. Then $\langle F\rangle$ becomes a common factor for all experiments on a given substrate, and the angular dependence is governed by the averaging of the remaining product over all hot spot axis orientations (i.e. over $\mathbf{e}_{HS}$). The treatment is then similar to that described in Ref. [19] for scattering by isotropically polarizable dipoles, but adapted here to uni-axial scatterers. For example, if we assume that the hot spot axes are randomly oriented in space, we deduce:

$$\begin{aligned} &I^{SS} = I\left(3M_I^S M_I^S\right),\quad I^{SP} = I\left(M_I^S M_R^P\right),\quad I^{PS} = I\left(M_I^P M_R^S\right),\\ &I^{PP} = I\left(2M_I^{P_{//}} M_R^{P_{//}} + 2M_I^{P_\perp} M_R^{P_\perp} + M_I^P M_R^P + M_I^{Px} M_R^{Px}\right) \end{aligned}, \tag{7}$$

where

$$I = \left(\langle F\rangle/15\right)\exp\left(-d/L_{IR}\right),\quad L_{IR} = 2\left[L(\lambda_I,\theta_I)^{-1} + L(\lambda_R,-\theta_R)^{-1}\right]^{-1}, \tag{8}$$

and for the incident light

$$\begin{aligned} &M_I^S = \left|E_y^S(\lambda_I,\theta_I)\right|^2,\quad M_I^{P_{//}} = \left|E_x^P(\lambda_I,\theta_I)\right|^2,\quad M_I^{P_\perp} = \left|E_z^P(\lambda_I,\theta_I)\right|^2,\\ &M_I^P = M_I^{P_{//}} + M_I^{P_\perp},\quad M_I^{Px} = 2\,\mathrm{Re}\left\{E_x^P(\lambda_I,\theta_I)\left(E_z^P(\lambda_I,\theta_I)\right)^*\right\} \end{aligned}, \tag{9}$$

with the same expressions for index R (Raman photons) replacing (λ_I,θ_I) by $(\lambda_R,-\theta_R)$.

These expressions can be applied to more complex interfaces, including multi-layers and absorptive materials, and similar expressions can be obtained for fluorescence [19]. For lossless media beyond critical angle as considered here, we moreover have $M_I^{Px} = 0$.

The predictions of this model are compared to the experimental results in Fig. 6. These are computed for a distance $d = 0$ from the interface, since the colloids producing the signal are on the interface (taking $d = 30$ nm, the typical radius of the colloid to account for the finite thickness, results in similar predictions not shown here). The detection angle dependence of the SERS signal is well explained by this model. The wide angular range observed here for SERS is a consequence of the fact that all the signals originate from a thin ($< L_{IR}$) layer on top of the interface. The evanescent coupling therefore remains good for all detection angles. This is in stark contrast with the experiments reported by Choi *et al.* on fluorescence [4]. In their case, the signal originated from every molecule excited by the incident field. The averaging of Eq. (7) over d then results in an additional factor proportional to L_{IR}. For excitation close to critical angle this factor decreases rapidly as the detection angle moves beyond the critical angle, explaining the dependence observed in Ref. [4].

The only fitting parameter of theoretical curves presented in Fig. 6 was the SERS signal intensity, since the experimental data was in arbitrary units. The same intensity value has been used for *SS*, *SP*, and *PS* polarization configurations. A notable discrepancy exists for the relative SERS signal intensity for the *PP* configuration which in the experiments was 5 times smaller than predicted. This can be attributed to the fact that the hot spot axes are not, in reality, randomly oriented, as we assumed when deriving Eqs. (7–9). One can see on SEM micrographs that silver clusters had a predominantly flat arrangement. A vertical axis would require two particles sitting on top of each other, a much less likely situation than two particles located side-by-side. However the procedure we have employed for SERS active

#102014 - $15.00 USD Received 26 Sep 2008; revised 11 Nov 2008; accepted 12 Nov 2008; published 21 Nov 2008

substrates preparation leaves no control over hot spot orientation. This prevents us from quantitatively accounting for this discrepancy in polarization dependence.

6. Conclusion

We have demonstrated the angular resolved detection of SERS signal from thiocyanate on aggregated silver nanoparticles beyond the critical angle at a glass-water interface. The extent of the angles accessible for observation is significantly wider compared with fluorescence detection in a similar geometry. This observation and the angular dependence can be explained by describing SERS hot spots as classical polarizable uni-axial dipoles radiating within a thin layer at the water side of the interface. The polarization dependence is shown to be specific to a particular hot spot orientation distribution. Our observations are generally applicable to SERS measurements using attenuated total reflection geometry.

Acknowledgment

This work was supported by NSF under Grant № ECS-0404002.

#102014 - $15.00 USD Received 26 Sep 2008; revised 11 Nov 2008; accepted 12 Nov 2008; published 21 Nov 2008